

**$b \rightarrow s\gamma$  decay in  $SU(2)_L \times SU(2)_R \times U(1)$  extensions of the standard model**

Peter Cho

*Lauritsen Laboratory, California Institute of Technology, Pasadena, California 91125*

Mikołaj Misiak

*Physik-Department, Technische Universität München, 85748 Garching, Germany*

(Received 25 October 1993)

The rare radiative decay  $b \rightarrow s\gamma$  is studied in  $SU(2)_L \times SU(2)_R \times U(1)$  extensions of the standard model. Matching conditions for coefficients of operators appearing in the low energy effective Hamiltonian for this process are derived, and QCD corrections to these coefficients are analyzed. The new contributions to the radiative transition which arise from the right-handed sector are suppressed by a small mixing angle. But this suppression is offset by a large  $m_t/m_b$  helicity flip factor and an enhanced matching condition coefficient function. We thus find that observable deviations from standard model predictions for the  $b \rightarrow s\gamma$  decay rate can occur in  $SU(2)_L \times SU(2)_R \times U(1)$  theories for a reasonable range of parameter values.

PACS number(s): 13.40.Hq, 12.15.Ji, 12.60.Cn

**I. INTRODUCTION**

The radiative weak decay  $b \rightarrow s\gamma$  has been the subject of significant experimental and theoretical study during the past several years. This rare transition has recently been observed for the first time in the exclusive channel  $\bar{B} \rightarrow K^*\gamma$  at CLEO [1]. The experimental bound on its inclusive rate has also been improved, and better limits are expected to be set within the next few years. On the theoretical side,  $b \rightarrow s\gamma$  decay is of considerable interest for several reasons. Firstly, since this process involves third generation fermions, it is sensitive to the heavy top quark, and its rate grows with increasing top mass. Secondly, strong interaction corrections to this weak radiative transition are known to be unusually large [2,3]. Two-loop diagrams that generate the leading QCD corrections to this decay actually dominate over the lowest-order one-loop graphs. But the most exciting feature of this transition is its potential to reveal departures from the standard model. Since flavor structure remains poorly understood, careful study of rare neutral flavor-changing processes offers one of the best prospects for glimpsing signs of new physics in the near future. The  $b \rightarrow s\gamma$  transition thus provides a window onto possible extensions of the standard model and has been investigated in two-Higgs-doublet models [4], supersymmetric theories [5], and extended technicolor scenarios [6]. Comparison of results from these theories with experimental measurements places constraints upon new physics which may lie beyond the standard model.

In this paper, we examine  $b \rightarrow s\gamma$  decay in another well-known extension of the standard model. Specifically, we consider theories based upon the extended electroweak gauge group  $SU(2)_L \times SU(2)_R \times U(1)$ . Such models have been widely studied in the past [7–9], and a number of phenomena such as  $K-\bar{K}$  mixing and neutrino masses have been used to constrain their allowed parameter spaces. The  $b \rightarrow s\gamma$  transition, however,

has received relatively little attention within the context of  $SU(2)_L \times SU(2)_R \times U(1)$  theories. We therefore will analyze this important rare process in these models and compare the results with those from the  $SU(2)_L \times U(1)_Y$  theory.

A previous study of the dominant gauge boson contributions to  $b \rightarrow s\gamma$  decay in  $SU(2)_L \times SU(2)_R \times U(1)$  theories has been reported in Ref. [10], while scalar contributions have been discussed in Ref. [11]. Our work differs from and improves upon these earlier findings in several important ways. Firstly, we perform our computations within the effective field theory framework which has become standard in  $b \rightarrow s\gamma$  investigations. Comparison of results between the  $SU(2)_L \times U(1)_Y$  and  $SU(2)_L \times SU(2)_R \times U(1)$  models is therefore facilitated. Use of effective field theory technology also allows us to systematically incorporate QCD running effects which have not been consistently treated before. Secondly, we do not restrict our analysis from the outset to models with manifest left-right symmetry as previous authors have done. Rather we allow for the more general case of asymmetrical left- and right-handed sectors. Finally, our results differ both qualitatively and quantitatively from those reported in the literature. We therefore believe that our findings provide several new insights into this problem.

Our paper is organized as follows. In Sec. II, we provide a general review of  $SU(2)_L \times SU(2)_R \times U(1)$  theories and present the particular model which forms the basis of our  $b \rightarrow s\gamma$  study. In Sec. III, we derive a low-energy effective theory starting from the full  $SU(2)_L \times SU(2)_R \times U(1)$  model, and we calculate the coefficients of the leading nonrenormalizable operators in its effective Hamiltonian which are relevant for  $b \rightarrow s\gamma$  decay. Strong interaction corrections are then discussed in Sec. IV. Finally, we evaluate the radiative decay rate for a range of reasonable parameter values in the

$SU(2)_L \times SU(2)_R \times U(1)$  theory and compare our results with those from the standard model.

## II. THE $SU(2)_L \times SU(2)_R \times U(1)$ MODEL

Theories based upon the electroweak gauge group  $SU(2)_L \times SU(2)_R \times U(1)$  represent well-known extensions of the standard model. Such theories have been widely investigated both as simple generalizations of the  $SU(2)_L \times U(1)_Y$  model and as possible intermediate stages in grand unified schemes such as  $SO(10)$ . One of the principle appeals of these models is that they allow for parity to be restored as a symmetry of nature at some energy scale above 250 GeV. A discrete left-right reflection has therefore commonly been imposed on most  $SU(2)_L \times SU(2)_R \times U(1)$  models which restricts their particle content and coupling constants. The incorporation of parity represents, however, an additional simplifying assumption which is not required by the structure of the extended electroweak gauge group. Moreover, left-right symmetric theories are known to encounter difficulties if considered in the context of grand unified models or cosmology [12,13]. So more recent studies have focused upon left-right asymmetric models. In this article, we will work within the framework of a general  $SU(2)_L \times SU(2)_R \times U(1)$  model and not impose left-right symmetry from the outset.

To begin, we combine the color and electroweak sectors and start with the extended gauge group  $G = SU(3)_C \times SU(2)_L \times SU(2)_R \times U(1)$ , which cascades down to the unbroken color and electromagnetic subgroup  $H = SU(3)_C \times U(1)_{EM}$  through the following simple symmetry-breaking pattern:

$$\begin{array}{cccc}
 SU(3)_C \times SU(2)_L \times SU(2)_R \times U(1) & & & \\
 T^a & T_L^i & T_R^i & S \\
 g_3 & g_{2L} & g_{2R} & g_1 \\
 & & \downarrow & \\
 SU(3)_C \times SU(2)_L \times U(1)_Y & & & \\
 T^a & T_L^i & Y/2 = T_R^3 + S & \\
 g_3 & g_{2L} & g' & \\
 & & \downarrow & \\
 SU(3)_C \times U(1)_{EM} & & & \\
 T^a & Q = T_L^3 + Y/2 & & \\
 g_3 & e. & & \\
 \end{array} \quad (2.1)$$

We have listed underneath each of the subgroup factors in this pattern our nomenclature conventions for their associated generators and coupling constants. Our covariant derivative with respect to the gauge group  $G$  thus appears as

$$\begin{aligned}
 D_\mu = & \partial_\mu + ig_3 G_\mu^a T^a + ig_{2L} W_{L\mu}^i T_L^i \\
 & + ig_{2R} W_{R\mu}^i T_R^i + ig_1 B_\mu S. \quad (2.2)
 \end{aligned}$$

We next display the fermion and scalar content of our model.<sup>1</sup> Quarks and leptons transform under  $G$  as

$$\begin{aligned}
 q'_L = \begin{bmatrix} u' \\ d' \end{bmatrix}_L & \sim (3, 2, 1)^{1/6}, & q'_R = \begin{bmatrix} u' \\ d' \end{bmatrix}_R & \sim (3, 1, 2)^{1/6}, \\
 l'_L = \begin{bmatrix} \nu' \\ e' \end{bmatrix}_L & \sim (1, 2, 1)^{-1/2}, & l'_R = \begin{bmatrix} \nu' \\ e' \end{bmatrix}_R & \sim (1, 1, 2)^{-1/2},
 \end{aligned} \quad (2.3)$$

where the primes indicate that these fields are gauge rather than mass eigenstates. The fermions also carry a suppressed generation index which ranges over three family values. We introduce the scalar field

$$\Phi = \begin{bmatrix} \phi_1^0 & \phi_1^+ \\ \phi_2^- & \phi_2^0 \end{bmatrix} \sim (1, 2, \bar{2})^0 \quad (2.4)$$

which acquires the complex vacuum expectation value (VEV)

$$\langle \Phi \rangle = \begin{bmatrix} k & 0 \\ 0 & k' \end{bmatrix} \quad (2.5)$$

and generates fermion masses in the Yukawa sector. After diagonalization of the quark mass matrices, the primed gauge eigenstate quark fields in (2.3) are related to unprimed mass eigenstate fields as

$$\begin{aligned}
 u'_L = S_u u_L, & \quad u'_R = T_u u_R, \\
 d'_L = S_d d_L, & \quad d'_R = T_d d_R,
 \end{aligned} \quad (2.6)$$

where  $S_{u,d}$  and  $T_{u,d}$  represent  $3 \times 3$  unitary matrices in family space.

We need to include additional Higgs fields into our theory in order to fully implement the symmetry-breaking pattern specified in (2.1). There are a number of possibilities for how these scalars may transform under  $G$ . The rate for  $b \rightarrow s\gamma$  decay in the  $SU(2)_L \times SU(2)_R \times U(1)$  model will not sensitively depend, however, upon the precise structure of its scalar sector. So we make the simplest choice and introduce two doublet fields,

$$\chi_L = \begin{bmatrix} \chi_L^+ \\ \chi_L^0 \end{bmatrix} \sim (1, 2, 1)^{1/2}, \quad \chi_R = \begin{bmatrix} \chi_R^+ \\ \chi_R^0 \end{bmatrix} \sim (1, 1, 2)^{1/2}, \quad (2.7)$$

which acquire the real VEV's

$$\langle \chi_L \rangle = \begin{bmatrix} 0 \\ v_L \end{bmatrix} \quad \text{and} \quad \langle \chi_R \rangle = \begin{bmatrix} 0 \\ v_R \end{bmatrix}. \quad (2.8)$$

Although  $\chi_L$  is not essential for symmetry-breaking purposes, we incorporate it along with  $\chi_R$  into the scalar sector so that our model can be rendered left-right symmetric if desired.

After the spontaneous symmetry breakdown  $G \rightarrow H$ , the kinetic energy terms in the scalar Lagrangian

$$\begin{aligned}
 \mathcal{L}_{\text{scalar}} = & \text{Tr}(D^\mu \Phi^\dagger D_\mu \Phi) + D^\mu \chi_L^\dagger D_\mu \chi_L \\
 & + D^\mu \chi_R^\dagger D_\mu \chi_R - V(\Phi, \chi_L, \chi_R) \quad (2.9)
 \end{aligned}$$

generate the charged  $W$  boson mass matrix

<sup>1</sup>Throughout the remainder of this section, we adopt notation which closely follows that established by Langacker and Sankar in Ref. [13].

$$M_{W^\pm}^2 = \begin{pmatrix} \frac{g_{2L}^2}{2}(v_L^2 + |k|^2 + |k'|^2) & -g_{2L}g_{2R}k^*k' \\ -g_{2L}g_{2R}kk'^* & \frac{g_{2R}^2}{2}(v_R^2 + |k|^2 + |k'|^2) \end{pmatrix} \equiv \begin{pmatrix} M_L^2 & M_{LR}^2 e^{i\alpha} \\ M_{LR}^2 e^{-i\alpha} & M_R^2 \end{pmatrix} \tag{2.10}$$

where  $\alpha$  represents the phase of  $k^*k'$ . The eigenvalues

$$\begin{aligned} M_1^2 &= M_L^2 \cos^2 \zeta + M_R^2 \sin^2 \zeta + M_{LR}^2 \sin 2\zeta, \\ M_2^2 &= M_L^2 \sin^2 \zeta + M_R^2 \cos^2 \zeta - M_{LR}^2 \sin 2\zeta, \end{aligned} \tag{2.11}$$

and eigenvectors

$$\begin{pmatrix} W_1^+ \\ W_2^+ \end{pmatrix} = \begin{pmatrix} \cos \zeta & e^{-i\alpha} \sin \zeta \\ -\sin \zeta & e^{-i\alpha} \cos \zeta \end{pmatrix} \begin{pmatrix} W_L^+ \\ W_R^+ \end{pmatrix} \tag{2.12}$$

of this mass matrix correspond to the physical charged  $W$  bosons in the  $SU(2)_L \times SU(2)_R \times U(1)$  theory. The mass  $M_2$  of the predominantly right-handed  $W_2$  as well as the small  $W_L$ - $W_R$  mixing angle defined by

$$\tan 2\zeta = -\frac{2M_{LR}^2}{M_R^2 - M_L^2} \tag{2.13}$$

are restricted by a number of low-energy phenomenological constraints. Numerical estimates for bounds on these quantities in left-right symmetric theories typically lie in the range [13,14]

$$M_2 > 1.4 \text{ TeV} \quad \text{and} \quad |\zeta| < 0.0025. \tag{2.14}$$

However, in some corners of parameter space in particular  $SU(2)_L \times SU(2)_R \times U(1)$  models,  $M_2$  masses as low as 300 GeV or mixing angles as large as  $|\zeta| \approx 0.013$  are allowed. So we will take the numbers in (2.14) as reasonable estimates for these two important parameters but consider ranges around these values as well.

In order to maintain explicit gauge invariance in our Green's functions, we will work in the background field version of 't Hooft–Feynman gauge [15]. The gauge-fixing Lagrangian in our model schematically appears as

$$\mathcal{L}_{GF} = -\frac{1}{2} \sum_a |\partial^\mu Q_\mu^a - g_a f^{abc} \bar{Q}_\mu^b Q^{\mu c} - ig_a (\phi^\dagger T^a \langle \phi \rangle - \langle \phi \rangle^\dagger T^a \phi)|^2. \tag{2.15}$$

Here  $Q_\mu^a$  represents a quantum gauge field for the gauge group  $G$ , while  $\bar{Q}_\mu^a$  stands for a classical background field for the unbroken subgroup  $H$ . As usual, the quadratic  $W_\mu \partial^\mu \phi$  cross terms that arise in the kinetic energy sector of the scalar Lagrangian (2.9) after spontaneous symmetry breaking are canceled by identical terms in the gauge-fixing Lagrangian. The expressions for the charged would-be Goldstone bosons corresponding to the longitudinal components of the physical  $W_{1,2}^+$  can simply be read off from these quadratic cross terms:

$$\begin{aligned} \pi_1^+ &= \frac{g_{2L}}{\sqrt{2}} \frac{\cos \zeta}{M_1} [(-k'^* + z_1 k^*)\phi_1^+ + (k - z_1 k')\phi_2^+ - v_L \chi_L^+ - z_1 v_R \chi_R^+], \\ \pi_2^+ &= \frac{g_{2R}}{\sqrt{2}} \frac{\cos \zeta}{M_2} e^{-i\alpha} [(k^* + z_2 k'^*)\phi_1^+ - (k' + z_2 k)\phi_2^+ + z_2 v_L \chi_L^+ - v_R \chi_R^+], \end{aligned} \tag{2.16}$$

where

$$z_1 = e^{-i\alpha} \frac{g_{2R}}{g_{2L}} \tan \zeta \quad \text{and} \quad z_2 = e^{i\alpha} \frac{g_{2L}}{g_{2R}} \tan \zeta. \tag{2.17}$$

In addition, the following trilinear interactions between the background photon field, physical  $W_{1,2}$  bosons and would-be Goldstone fields in the gauge-fixing Lagrangian

$$\mathcal{L}_{GF} = \dots + eM_1 \bar{A} W_1^+ \pi_1^- + eM_2 \bar{A} W_2^+ \pi_2^- + \text{H.c.} \tag{2.18}$$

are also canceled by terms in the Higgs kinetic energy sector. This extra cancellation results from our particular choice of 't Hooft–Feynman background field gauge and will simplify our  $b \rightarrow s\gamma$  analysis.

Having identified the Goldstone fields in Eq. (2.16), we can readily derive their charged current interactions. It is important to note that the form of these interactions is independent of our particular choice of scalar representations in this model. We display below the terms in the charged current Lagrangian which are relevant for  $b \rightarrow s\gamma$  decay:

$$\begin{aligned}
\mathcal{L}_{CC} = & \frac{1}{\sqrt{2}}(\bar{u} \bar{c} \bar{t}) \{ W_1^+ [ -g_{2L} \cos\zeta V_L P_- - g_{2R} \sin\zeta e^{i\alpha} V_R P_+ ] + W_2^+ [ g_{2L} \sin\zeta V_L P_- - g_{2R} \cos\zeta e^{i\alpha} V_R P_+ ] \\
& + \frac{\pi_1^+}{M_1} [ (g_{2L} \cos\zeta V_L M_D - g_{2R} e^{i\alpha} \sin\zeta M_U V_R) P_+ - (g_{2L} \cos\zeta M_U V_L - g_{2R} e^{i\alpha} \sin\zeta V_R M_D) P_- ] \\
& + \frac{\pi_2^+}{M_2} [ -(g_{2L} \sin\zeta V_L M_D + g_{2R} e^{i\alpha} \cos\zeta M_U V_R) P_+ \\
& + (g_{2L} \sin\zeta M_U V_L + g_{2R} e^{i\alpha} \cos\zeta V_R M_D) P_- ] \} \begin{pmatrix} d \\ s \\ b \end{pmatrix} + \text{H.c.} + \dots . \quad (2.19)
\end{aligned}$$

In this expression,  $P_{\pm} = (1 \pm \gamma^5)/2$  represent right- and left-handed projection operators,  $M_U$  and  $M_D$  denote the diagonalized quark mass matrices

$$M_U = \begin{pmatrix} m_u & 0 & 0 \\ 0 & m_c & 0 \\ 0 & 0 & m_t \end{pmatrix}, \quad M_D = \begin{pmatrix} m_d & 0 & 0 \\ 0 & m_s & 0 \\ 0 & 0 & m_b \end{pmatrix}, \quad (2.20)$$

and  $V_L = S_u^\dagger S_d$  and  $V_R = T_u^\dagger T_d$  are the left- and right-handed analogs of the Kobayashi-Maskawa (KM) matrices in the  $SU(2)_L \times SU(2)_R \times U(1)$  model. In left-right symmetric theories, these KM matrices are related as  $|V_L| = |V_R|$  which clearly reduces the number of free parameters.

### III. THE EFFECTIVE THEORY

The rare decay  $b \rightarrow s\gamma$  is sensitive to new physics above the electroweak scale  $v_L$ . In most  $SU(2)_L \times SU(2)_R \times U(1)$  extensions of the standard model, the separation between  $v_L$  and the scale  $v_R$  where the gauge group  $G$  spontaneously breaks is quite large. The difference between the bottom quark and electroweak scales is also large. Therefore, this low-energy radiative transition is especially well suited for analysis within an effective field theory framework which can take advantage of these large scale separations.

The construction of the effective theory begins at  $\mu = v_R$  in the  $SU(2)_L \times SU(2)_R \times U(1)$  model. Fields with masses of order this scale are integrated out, but their virtual effects are incorporated into nonrenormalizable operators whose coefficients are suppressed by powers of  $1/v_R$ . Since the lower bound on  $v_R$  lies in the multihundred GeV region, the contributions from  $W_2^\pm$  and charged physical scalars, which naturally have  $\mathcal{O}(v_R)$  masses, to  $b \rightarrow s\gamma$  mediating operators are very small compared to those from  $W_1^\pm$ . We therefore ignore such contributions and jump down to the  $W_1$  scale where we simultaneously integrate out the top quark and charged intermediate boson. Our neglect of the splitting between the top and  $W_1$  introduces an error. However, its magnitude is known to be approximately 10% in the standard

model [16], and we expect its size in the  $SU(2)_L \times SU(2)_R \times U(1)$  theory to be comparable. We therefore will tolerate this small uncertainty which could be systematically refined if desired.

The dominant one-loop contributions to  $b \rightarrow s\gamma$  in the  $SU(2)_L \times SU(2)_R \times U(1)$  model come from the diagrams displayed in Fig. 1. We evaluate these graphs with their external propagators placed on shell. After performing an operator product expansion, we extract the leading terms which match onto local magnetic moment operators. Such terms are generated only by the four one-particle irreducible (1PI) diagrams shown in the figure. Other one-particle reducible (1PR) graphs which arise at one-loop order do not match onto magnetic moment operators and may therefore be ignored.

It is sensible to make some simplifications at this stage. First, since  $\zeta$  is known to be quite small compared to unity, we work only to  $\mathcal{O}(\zeta)$  and set  $\cos\zeta \rightarrow 1$  and  $\sin\zeta \rightarrow \zeta$ . Moreover, since  $\zeta$  will always appear in combination with  $g_{2R}/g_{2L}$ , we define  $\zeta_g = g_{2R}/g_{2L}\zeta$ . We also neglect the mass of the strange quark relative to the bottom quark mass. The  $b \rightarrow s\gamma$  amplitude is then given at the  $W_1$  scale by the *tree level* matrix element of the effective Hamiltonian

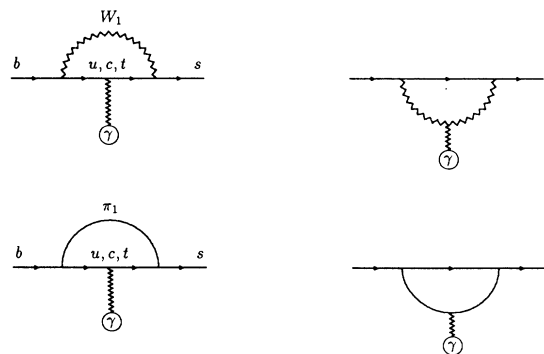


FIG. 1. One-loop 1PI intermediate gauge and would-be Goldstone boson graphs which contribute to the  $b \rightarrow s\gamma$  matching condition at the  $W_1$  scale. The circles at the ends of wavy external propagators represent background photon fields.

$$H_{\text{eff}} = -\frac{4G_F}{\sqrt{2}} \frac{em_b}{16\pi^2} \sum_{i=u,c,t} V_L^{is*} V_L^{ib} \left\{ F(x_i) \bar{s} \sigma^{\mu\nu} P_+ b F_{\mu\nu} + \zeta_g \frac{m_i}{m_b} \tilde{F}(x_i) \bar{s} \sigma^{\mu\nu} \left[ \frac{V_R^{ib}}{V_L^{ib}} e^{i\alpha} P_+ + \left( \frac{V_R^{is}}{V_L^{is}} \right)^* e^{-i\alpha} P_- \right] b F_{\mu\nu} \right\}. \quad (3.1)$$

where  $x_i = (m_i/M_{W_1})^2$  and

$$\begin{aligned} F(x) &= \frac{x(7-5x-8x^2)}{24(x-1)^3} - \frac{x^2(2-3x)}{4(x-1)^4} \ln x, \\ \tilde{F}(x) &= \frac{-20+31x-5x^2}{12(x-1)^2} + \frac{x(2-3x)}{2(x-1)^3} \ln x. \end{aligned} \quad (3.2)$$

The first term inside the curly brackets in (3.1) is precisely the same as in the standard model to which the  $SU(2)_L \times SU(2)_R \times U(1)$  theory reduces in the limit  $v_R \rightarrow \infty$ . Its coefficient function  $F$  is identical to the analogous standard model function which was first calculated by Inami and Lim [17]. On the other hand, the second term proportional to  $\tilde{F}$  represents a qualitatively new contribution to  $H_{\text{eff}}$ . Since the physical  $W_1$  boson in the  $SU(2)_L \times SU(2)_R \times U(1)$  theory couples to both left- and right-handed quarks, the one-loop diagrams in Fig. 1 can directly match onto odd dimension operators if the intermediate charge  $\frac{2}{3}$  quarks in these graphs undergo a helicity flip. The new terms arising from the  $SU(2)_L \times SU(2)_R \times U(1)$  theory are therefore proportional to  $m_{i=u,c,t}$  rather than  $m_b$ . Of course, the contribution coming from the virtual top quark is the most important, since it enhances the second term in Eq. (3.1) relative to the first by  $m_t/m_b$ . This contribution is further enlarged by the ratio  $r = \tilde{F}(x_t)/F(x_t)$ , which ranges over the interval  $7.7 \geq r \geq 3.5$  for  $100 \text{ GeV} \leq m_t \leq 200 \text{ GeV}$ . So these two effects offset the suppression of the second term in (3.1) by the small mixing angle  $\zeta_g$ . It is important to note that no such enhancement occurs in the leading terms of diagrams such as those in Fig. 1 with  $W_1$  replaced by  $W_2$ . So although  $W_L$ - $W_R$  mixing and  $W_2$  exchange are both  $O(1/v_R^2)$  effects, the impact of the

former upon  $b \rightarrow s\gamma$  decay in the  $SU(2)_L \times SU(2)_R \times U(1)$  model is much more important than the latter.

Our matching results differ from those reported previously by Cocolicchio *et al.* in Ref. [10]. In order to compare, we have calculated all the necessary one-loop diagrams in ordinary as well as background field 't Hooft-Feynman gauge. The expressions we have obtained for the one-loop  $W_1$  boson graphs in the ordinary gauge are equivalent to the functions  $F_{2\gamma a}^{LR}(x)$  and  $F_{2\gamma b}^{LR}(x)$  in Eq. (17) of Ref. [10]. However, the contributions from the would-be Goldstone diagrams, which we have explicitly calculated, disagree with the  $F_{2\gamma c}^{LR}(x)$  results of Cocolicchio *et al.* Their sum  $F_{2\gamma a}^{LR} + F_{2\gamma b}^{LR} + F_{2\gamma c}^{LR}$  differs qualitatively and quantitatively from our function  $\tilde{F}(x)$ .

Having found the effective Hamiltonian expression in (3.1), we can easily take its tree level matrix element and compute the  $b \rightarrow s\gamma$  decay rate:

$$\Gamma(b \rightarrow s\gamma) = \frac{G_F^2 m_b^5}{32\pi^4} \alpha_{\text{EM}}(m_b) (|C|^2 + |C'|^2), \quad (3.3)$$

where

$$\begin{aligned} C &= \sum_{i=u,c,t} V_L^{is*} V_L^{ib} \left[ F(x_i) + \zeta_g \frac{m_i}{m_b} \tilde{F}(x_i) \frac{V_R^{ib}}{V_L^{ib}} e^{i\alpha} \right], \\ C' &= \sum_{i=u,c,t} V_L^{is*} V_L^{ib} \left[ \zeta_b \frac{m_i}{m_b} \tilde{F}(x_i) \left( \frac{V_R^{is}}{V_L^{is}} \right)^* e^{-i\alpha} \right]. \end{aligned} \quad (3.4)$$

It is common practice to normalize this radiative partial width to the semileptonic rate

$$\Gamma(b \rightarrow ce\bar{\nu}_e) = \frac{G_F^2 m_b^5}{192\pi^3} |V_L^{cb}|^2 g(m_c/m_b), \quad (3.5)$$

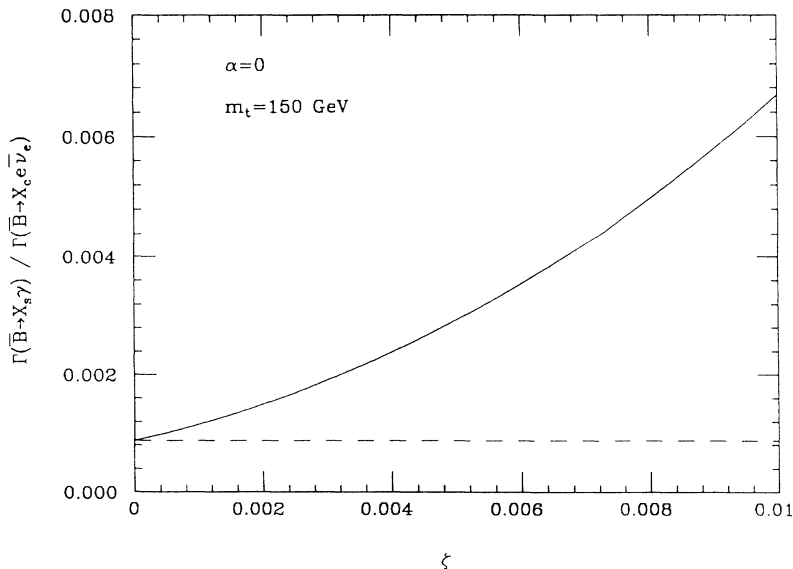


FIG. 2. Inclusive  $\bar{B} \rightarrow X_s \gamma$  decay rate normalized to the semileptonic  $\bar{B} \rightarrow X_c e \bar{\nu}_e$  rate plotted as a function of the mixing angle  $\zeta$  with  $m_t = 150 \text{ GeV}$  and  $\alpha = 0$ . The solid and dashed curves depict the QCD uncorrected results in  $SU(2)_L \times SU(2)_R \times U(1)$  theory and the standard model, respectively.

where  $g(\epsilon) = 1 - 8\epsilon^2 - 24\epsilon^4 \ln \epsilon + 8\epsilon^6 - \epsilon^8$  represents a phase-space factor [18]. The sensitive dependence of Eqs. (3.3) and (3.5) upon the bottom quark mass and the KM angles then cancels in their ratio

$$R \equiv \frac{\Gamma(b \rightarrow s\gamma)}{\Gamma(b \rightarrow ce\bar{\nu}_e)} \simeq \frac{\Gamma(\bar{B} \rightarrow X_s \gamma)}{\Gamma(\bar{B} \rightarrow X_c e \bar{\nu}_e)}. \quad (3.6)$$

This ratio is plotted in Fig. 2 as a function of the mixing angle  $\zeta$  with the top mass  $m_t = 150$  GeV and phase angle  $\alpha = 0$  held fixed,  $g_{2L}$  set equal to  $g_{2R}$ , and all ratios of left- and right-handed KM angles set equal to unity. In this left-right symmetric limit, the up and charm quark contributions to the coefficients in (3.4) are completely negligible. As can be seen in the figure, the QCD uncorrected  $b \rightarrow s\gamma$  rate in the  $SU(2)_L \times SU(2)_R \times U(1)$  model is twice that in the standard model for the canonical value  $\zeta = 0.0025$ . The rate is of course even larger for greater values of  $\zeta$ . We therefore see that the new contributions to the low-energy effective Hamiltonian from the  $SU(2)_L \times SU(2)_R \times U(1)$  theory can lead to significant deviations from the  $b \rightarrow s\gamma$  predictions of the standard model.

#### IV. STRONG INTERACTION CORRECTIONS

QCD corrections to  $b \rightarrow s\gamma$  decay have received considerable attention during the past several years and are known to be very large in the standard model [2,3]. The analysis of strong interaction effects upon the rare radiative transition is most sensibly conducted within the five-quark effective theory where large logarithms can be summed using the renormalization group. Since the structure of the low-energy effective theory does not sensitively depend upon the precise nature of physics beyond the electroweak scale, the computation of strong interaction corrections is similar in both the  $SU(2)_L \times SU(2)_R \times U(1)$  and  $SU(2)_L \times U(1)_Y$  models. We can therefore take over many well-known results from prior  $b \rightarrow s\gamma$  studies.

We start by generalizing the effective Hamiltonian in (3.1) to include operators that mix with the photon magnetic moment terms under the action of QCD renormalization:

$$H_{\text{eff}} = -\frac{4G_F}{\sqrt{2}} V_L^{ts*} V_L^{tb} \sum_j C_j(\mu) O_j(\mu). \quad (4.1)$$

We adopt the following conventional choice for the set of operators appearing in the effective Hamiltonian:

$$\begin{aligned} O_1 &= (\bar{s}_\alpha \gamma_\mu P - c^\beta)(\bar{c}_\beta \gamma^\mu P - b^\alpha), \\ O_2 &= (\bar{s}_\alpha \gamma_\mu P - c^\alpha)(\bar{c}_\beta \gamma^\mu P - b^\beta), \\ O_3 &= (\bar{s}_\alpha \gamma_\mu P - b^\alpha) \sum_q (\bar{q}_\beta \gamma^\mu P - q^\beta), \\ O_4 &= (\bar{s}_\alpha \gamma_\mu P - b^\beta) \sum_q (\bar{q}_\beta \gamma^\mu P - q^\alpha), \\ O_5 &= (\bar{s}_\alpha \gamma_\mu P - b^\alpha) \sum_q (\bar{q}_\beta \gamma^\mu P + q^\beta), \end{aligned} \quad (4.2)$$

$$O_6 = (\bar{s}_\alpha \gamma_\mu P - b^\beta) \sum_q (\bar{q}_\beta \gamma^\mu P + q^\alpha),$$

$$O_7 = \frac{e}{16\pi^2} m_b \bar{s}_\alpha \sigma^{\mu\nu} P + b^\alpha F_{\mu\nu},$$

$$O_8 = \frac{g_3}{16\pi^2} m_b \bar{s}_\alpha \sigma^{\mu\nu} P + (T^a)_\beta^\alpha b^\beta G_{\mu\nu}^a.$$

Here  $\alpha$  and  $\beta$  represent color indices, while the summation over  $q$  ranges over the five active quark flavors. This list constitutes a complete operator basis if the underlying full theory is the standard, two-Higgs doublet or minimal supersymmetric model.

In the  $SU(2)_L \times SU(2)_R \times U(1)$  effective theory, however, new operators with different chirality structures can arise. In particular, we need to include the four-quark terms

$$\begin{aligned} O_9 &= \left[ \frac{m_b}{m_c} \right] (\bar{s}_\alpha \gamma_\mu P - c^\beta)(\bar{c}_\beta \gamma^\mu P + b^\alpha), \\ O_{10} &= \left[ \frac{m_b}{m_c} \right] (\bar{s}_\alpha \gamma_\mu P - c^\alpha)(\bar{c}_\beta \gamma^\mu P + b^\beta), \end{aligned} \quad (4.3)$$

which are left-right analogues of  $O_1$  and  $O_2$ . The ratios of the bottom and charm quark masses are incorporated into their definitions to facilitate later mixing computations involving these operators. We also need to introduce the flipped chirality partners  $O'_1 - O'_{10}$  of  $O_1 - O_{10}$  obtained by setting  $P_\pm \rightarrow P_\mp$  in Eqs. (4.2) and (4.3). Most of these new operators will fortunately play no significant role in our  $b \rightarrow s\gamma$  analysis. So the total number of operators that we will actually need to consider is much smaller than 20.

After performing a straightforward matching computation, we find the following  $W_1$  scale coefficient values in the limit of vanishing up quark mass:<sup>2</sup>

$$\begin{aligned} C_2(M_{W_1}) &= 1, \quad C'_2(M_{W_1}) = 0, \\ C_7(M_{W_1}) &= F(x_t) + A^{tb} \bar{F}(x_t) + A^{cb}, \\ C'_7(M_{W_1}) &= (A^{ts})^* \bar{F}(x_t) + (A^{cs})^*, \\ C_8(M_{W_1}) &= G(x_t) + A^{tb} \bar{G}(x_t), \\ C'_8(M_{W_1}) &= (A^{ts})^* \bar{G}(x_t), \\ C_{10}(M_{W_1}) &= A^{cb}, \quad C'_{10}(M_{W_1}) = (A^{cs})^*, \end{aligned} \quad (4.4)$$

where

$$A^{UD} = \zeta_g \frac{m_U}{m_b} \frac{V_R^{UD}}{V_L^{UD}} e^{i\alpha} \quad \text{for } U = u, c, t \quad \text{and } D = d, s, b. \quad (4.5)$$

<sup>2</sup>We retain the charm quark contributions to (4.4) even though they are suppressed relative to the top quark terms by  $m_c/m_t$ . This small factor could in principle be offset by the ratio of KM angles in (4.5) in an asymmetric left-right model.

The functions  $F$  and  $\tilde{F}$  in the coefficients of the photon magnetic moment operators  $O_7^{(\prime)}$  were previously specified in (3.2). The analogous functions for the gluon magnetic moment operators  $O_8^{(\prime)}$  are given by

$$\begin{aligned} G(x) &= \frac{x(2+5x-x^2)}{8(x-1)^3} - \frac{3x^2}{4(x-1)^4} \ln x, \\ \tilde{G}(x) &= -\frac{4+x+x^2}{4(x-1)^2} + \frac{3x}{2(x-1)^3} \ln x. \end{aligned} \quad (4.6)$$

All other operator coefficients vanish at the  $W_1$  scale.

The renormalization-group mixing of the operators in our basis set is governed by a  $20 \times 20$  anomalous dimension matrix  $\gamma$ . Since the strong interactions preserve chirality, the unprimed operators in Eqs. (4.2) and (4.3) cannot mix with their primed counterparts under the action of QCD. Moreover, renormalization-group mixing within the two separate operator sectors is precisely the same. Therefore,  $\gamma$  decomposes into two identical  $10 \times 10$  blocks. The leading order structure of these blocks breaks up into an  $8 \times 8$  submatrix  $\gamma_{8 \times 8}$  and a partially overlapping  $4 \times 4$  submatrix  $\gamma_{4 \times 4}$ . The  $8 \times 8$  matrix describes the mixing among  $O_1^{(\prime)} - O_8^{(\prime)}$  and has been calculated by a number of groups [2,3]. At this time, complete consensus regarding the exact values for all the entries in  $\gamma_{8 \times 8}$  has not been achieved. While this lack of agreement is disturbing, it is of relatively little practical importance, since all competing claims for  $\gamma_{8 \times 8}$  yield nearly identical numerical results for the  $b \rightarrow s\gamma$  decay rates in the  $SU(2)_L \times U(1)_Y$  and  $SU(2)_L \times SU(2)_R \times U(1)$  models. We will use the recent results of Ciuchini *et al.* for this matrix. The remaining  $4 \times 4$  matrix overlaps with

$\gamma_{8 \times 8}$  and controls the mixing of the two new four-quark operators in (4.3) into the dimension-five photon and gluon magnetic moment operators. Its entries can be extracted from the computations of analogous mixings within  $\gamma_{8 \times 8}$  and are exhibited below:

$$\gamma_{4 \times 4} = \begin{matrix} O_7^{(\prime)} & O_8^{(\prime)} & O_9^{(\prime)} & O_{10}^{(\prime)} \\ \left[ \begin{array}{cccc} 16/3 & 0 & 0 & 0 \\ -16/9 & 14/3 & 0 & 0 \\ 80/3 & -2 & -8 & 0 \\ 32/9 & 4/3 & -3 & 1 \end{array} \right] & \frac{g_3^2}{8\pi^2} \end{matrix}. \quad (4.7)$$

All other entries in the  $10 \times 10$  anomalous dimension blocks vanish.

Once the anomalous dimension matrix is determined, it is straightforward to solve the renormalization group equation which relates coefficient values at  $\mu = M_{W_1}$  to those at  $\mu = m_b$ . The solution appears as

$$C_i(m_b) = \sum_{j,k} (S^{-1})_{ij} (\eta^{3\lambda_j/23}) S_{jk} C_k(M_{W_1}) \quad (4.8)$$

where the  $\lambda_j$ 's in the exponent of  $\eta = \alpha_s(M_{W_1})/\alpha_s(m_b)$  are the eigenvalues of  $\hat{\gamma} = \gamma/(g_3^2/8\pi^2)$  and the rows of matrix  $S$  contain the corresponding eigenvectors.

Assembling together the bottom scale coefficients and matrix elements of all the operators in our basis set, we finally obtain the QCD corrected  $b \rightarrow s\gamma$  decay rate in the  $SU(2)_L \times SU(2)_R \times U(1)$  model:

$$\Gamma(b \rightarrow s\gamma) = \frac{G_F^2 m_b^5}{32\pi^4} \alpha_{EM}(m_b) |V_L^{ts} V_L^{tb}|^2 (|C_{7\text{eff}}(m_b)|^2 + |C'_{7\text{eff}}(m_b)|^2). \quad (4.9)$$

The effective magnetic moment operator coefficients are given by

$$\begin{aligned} C_{7\text{eff}}(m_b) &= C_{7\text{eff}}(m_b)_{\text{SM}} + A^{tb} [\eta^{16/23} \tilde{F}(x_t) + \frac{8}{3}(\eta^{14/23} - \eta^{16/23}) \tilde{G}(x_t)] + A^{cb} \sum_{i=1}^4 h_i' \eta^{p_i'}, \\ C'_{7\text{eff}}(m_b) &= (A^{ts})^* [\eta^{16/23} \tilde{F}(x_t) + \frac{8}{3}(\eta^{14/23} - \eta^{16/23}) \tilde{G}(x_t)] + (A^{cs})^* \sum_{i=1}^4 h_i' \eta^{p_i'}, \end{aligned} \quad (4.10)$$

where

$$C_{7\text{eff}}(m_b)_{\text{SM}} = \eta^{16/23} F(x_t) + \frac{8}{3}(\eta^{14/23} - \eta^{16/23}) G(x_t) + \sum_{i=1}^8 h_i \eta^{p_i} \quad (4.11)$$

denotes the corresponding standard model result. The coefficients  $h_i$  and powers  $p_i$  entering into the last term have been discussed and tabulated in the Appendix of Ref. [19]. We simply quote them here

$$\begin{aligned} (h_1, h_2, h_3, h_4, h_5, h_6, h_7, h_8) &= (2.2996, -1.0880, -0.4286, -0.0714, -0.6494, -0.0380, -0.0186, -0.0057), \\ (p_1, p_2, p_3, p_4, p_5, p_6, p_7, p_8) &= (0.6087, 0.6957, 0.2609, -0.5217, 0.4086, -0.4230, -0.8994, 0.1456), \end{aligned} \quad (4.12)$$

along with the  $h_i'$  and  $p_i'$  values

$$\begin{aligned} (h_1', h_2', h_3', h_4') &= (-0.6615, 1.3142, 0.0070, 1.0070), \\ (p_1', p_2', p_3', p_4') &= (0.6957, 0.6087, -1.0435, 0.1304). \end{aligned} \quad (4.13)$$

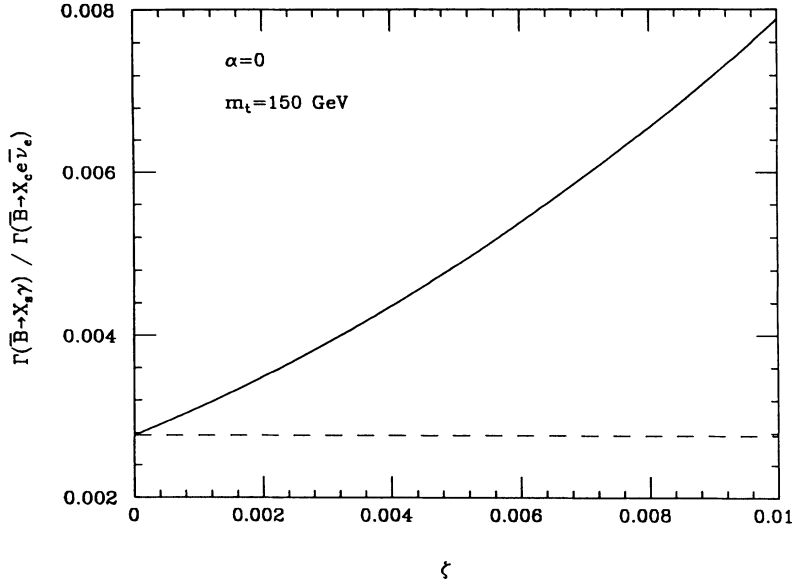


FIG. 3. Inclusive  $\bar{B} \rightarrow X_s \gamma$  decay rate normalized to the semileptonic  $\bar{B} \rightarrow X_c e \bar{\nu}_e$  rate plotted as a function of the mixing angle  $\zeta$  with  $m_t = 150$  Ge and  $\alpha = 0$ . The solid and dashed curves depict the QCD corrected results in  $SU(2)_L \times SU(2)_R \times U(1)$  theory and the standard model, respectively.

The radiative partial width in (4.9) is regularization and renormalization scheme independent as must be the case for any physical observable.<sup>3</sup> We normalize it to the QCD corrected generalization of the semileptonic rate in (3.5),

$$\Gamma(b \rightarrow ce\bar{\nu}_e) = \frac{G_F^2 m_b^5}{192\pi^3} |V_L^{cb}|^2 g(m_c/m_b) \left[ 1 - \frac{2}{3\pi} \alpha_s(m_b) f(m_c/m_b) \right], \quad (4.14)$$

and form the ratio

$$R = \frac{\Gamma(b \rightarrow s\gamma)}{\Gamma(b \rightarrow ce\bar{\nu}_e)} \simeq \frac{\Gamma(\bar{B} \rightarrow X_s \gamma)}{\Gamma(\bar{B} \rightarrow X_c e \bar{\nu}_e)} = \frac{6}{\pi} \frac{\alpha_{EM}(m_b)}{g(m_c/m_b)} \frac{|C_7(m_b)_{\text{eff}}|^2 + |C_7'(m_b)_{\text{eff}}|^2}{1 - \frac{2}{3\pi} \alpha_s(m_b) f(m_c/m_b)}. \quad (4.15)$$

The function  $f$  appearing in these expressions encodes sizable next-to-leading-order strong interaction effects, which we choose to include and is numerically tabulated in Ref. [18]. In order to restrict the parameter dependence of  $R$  so that it can be simply displayed, we will specialize to the left-right symmetric limit and set  $g_{2L} = g_{2R}$  and  $|V_L| = |V_R|$ .  $R$  then depends only upon the three parameters  $\zeta$ ,  $m_t$ , and  $\alpha$ .

In Fig. 3, we plot  $R$  as a function of the mixing angle  $\zeta$  in both the  $SU(2)_L \times SU(2)_R \times U(1)$  and  $SU(2)_L \times U(1)_Y$  models with  $m_t = 150$  GeV and  $\alpha = 0$  held fixed.<sup>4</sup> Comparing these curves with their QCD uncorrected counterparts in Fig. 2, we see that the strong interactions triple the  $b \rightarrow s\gamma$  rate for very small values of  $\zeta$ . The strong interaction enhancement at larger values of  $\zeta$  is less pronounced. The reason behind this trend can be seen in the expressions for the effective photon magnetic moment coefficients  $C_{7\text{eff}}^{(\prime)}(m_b)$  and  $C_{7\text{eff}}(m_b)_{\text{SM}}$ . Recall that the disparity between these coefficients stems mainly from

the terms proportional to  $\tilde{F}(x_i)$  in (4.10). This discrepancy is suppressed, however, by the QCD factor  $\eta^{16/23} = 0.67$ . The last term in (4.11) overcomes this suppression factor and leads to a net QCD enhancement of the  $b \rightarrow s\gamma$  rate in both the  $SU(2)_L \times SU(2)_R \times U(1)$  and  $SU(2)_L \times U(1)_Y$  models. But the strong interactions tend to diminish the difference between these two theories' rates.

The dependence of  $R$  upon  $m_t$  for  $\zeta = 0.0025$  and  $\alpha = 0$  is illustrated in Fig. 4. Both the  $SU(2)_L \times SU(2)_R \times U(1)$  theory and standard model results grow with increasing top mass. For all  $m_t$  above the present experimental lower bound of 131 GeV [20], we see that the former is greater than the latter by at least 30% for this choice of parameters. Such a variation is potentially large enough to differentiate between these two models given current theoretical and future experimental uncertainties. Other regions in parameter space can of course yield larger or smaller discrepancies. We believe, however, that the re-

<sup>3</sup>We should point out that the coefficients  $C_7^{(\prime)}$  and  $C_8^{(\prime)}$  in Eq. (4.4), the nonvanishing off-diagonal  $2 \times 2$  block in the anomalous dimension submatrix  $\gamma_{4 \times 4}$  in Eq. (4.7), and the one-loop matrix elements of  $O_9^{(\prime)}$  and  $O_{10}^{(\prime)}$  are regularization scheme dependent. These quantities were all calculated in the fully anticommuting  $\gamma^5$  dimensional regularization scheme.

<sup>4</sup>The graph in Fig. 3 may be interpreted in the context of an asymmetric left-right model by rescaling  $\zeta \rightarrow \zeta_g |V_R/V_L|$  provided  $|A^{tb}| = |A^{ts}| \gg |A^{cb}|, |A^{cs}|$ .

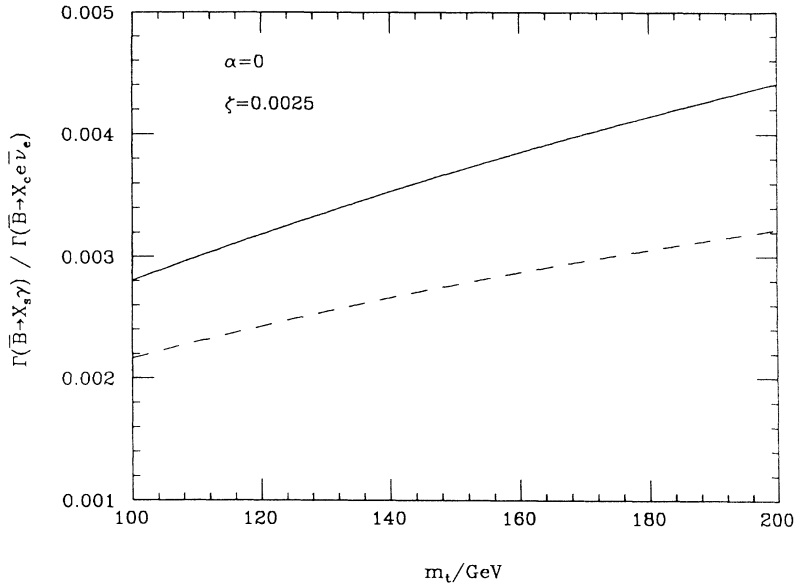


FIG. 4. Inclusive  $\bar{B} \rightarrow X_s \gamma$  decay rate normalized to the semileptonic  $\bar{B} \rightarrow X_c e \bar{\nu}_e$  rate plotted as a function of the top quark mass  $m_t$  with  $\zeta=0.0025$  and  $\alpha=0$ . The solid and dashed curves depict the QCD corrected results in  $SU(2)_L \times SU(2)_R \times U(1)$  theory and the standard model, respectively.

sults in Fig. 4 are representative for most left-right symmetric models.

Finally, we plot  $R$  as a function of the phase angle  $\alpha$  with  $\zeta=0.0025$  and  $m_t=150$  GeV held fixed in Fig. 5. As can be seen in the graph, maximum constructive and destructive interference between the standard model and  $SU(2)_L \times SU(2)_R \times U(1)$  contributions to the  $b \rightarrow s \gamma$  effective Hamiltonian occur for  $\alpha=0$  and  $\pi$ , respectively. Distinguishing between the two theories is consequently easiest for values of  $\alpha$  near these two end points. Such values are fortunately favored in the  $SU(2)_L \times SU(2)_R \times U(1)$  model to avoid excessive  $CP$  violation [13].

In conclusion, we have analyzed the rare  $b \rightarrow s \gamma$  decay mode in  $SU(2)_L \times SU(2)_R \times U(1)$  extensions of the standard model. We have found that mixing between left and right  $W$  bosons in such models can lead to sizable new

contributions to the effective Hamiltonian for this radiative process even though the mixing angle  $\zeta$  is constrained to be quite small. QCD corrections diminish the disparity between the  $b \rightarrow s \gamma$  rates in the  $SU(2)_L \times SU(2)_R \times U(1)$  and  $SU(2)_L \times U(1)_Y$  theories. However, for reasonable ranges of parameter values, the decay rates can be distinguished and used to probe for new physics beyond the standard model.

*Note added.* After this paper was submitted for publication, we learned that work on a similar topic was simultaneously reported by Fujikawa and Yamada in Ref. [21]. The basic results of these authors are consistent with the findings presented here.

#### ACKNOWLEDGMENTS

We thank Andrzej Buras and Mark Wise for helpful discussions. P.C. thanks the Aspen Center for Physics

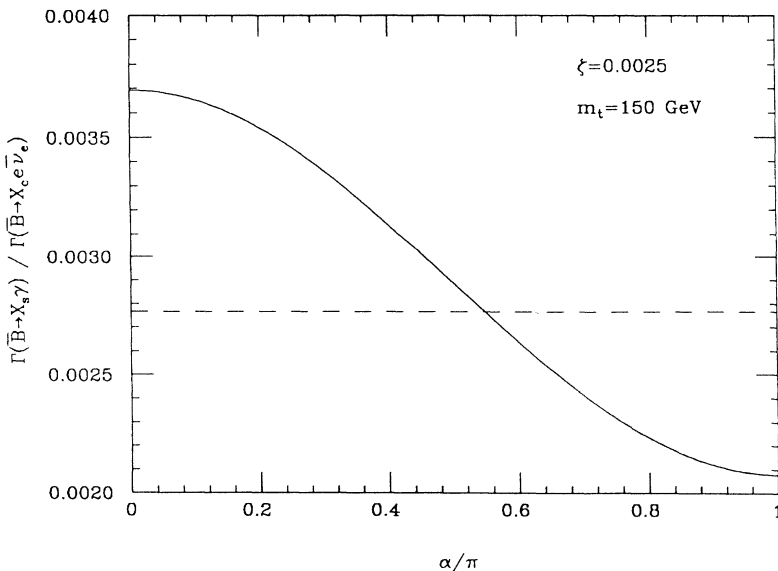


FIG. 5. Inclusive  $\bar{B} \rightarrow X_s \gamma$  decay rate normalized to the semileptonic  $\bar{B} \rightarrow X_c e \bar{\nu}_e$  rate plotted as a function of the phase angle  $\alpha$  with  $\zeta=0.0025$  and  $m_t=150$  GeV. The solid and dashed curves depict the QCD corrected results in  $SU(2)_L \times SU(2)_R \times U(1)$  theory and the standard model, respectively.

and the high-energy theory group at Technische Universität München, where work on this paper was performed, for their warm hospitality. The work of P.C. was supported in part by the U.S. Dept. of Energy under DOE Grant No. PDE-FG03-92ER40701, the CEC Sci-

ence Project SC1-CT91-0729, and the SSC Laboratory. The work of M.M. was supported in part by the German Bundesministerium für Forschung und Technologie under Contract No. 06 TM 732 and by the Polish Committee for Scientific Research.

- 
- [1] CLEO Collaboration, R. Ammar *et al.*, Phys. Rev. Lett. **71**, 674 (1993).
  - [2] B. Grinstein, R. Springer, and M. B. Wise, Nucl. Phys. **B339**, 269 (1990); M. Misiak, *ibid.* **B393**, 23 (1993); R. Grigjanis, P. J. O'Donnell, M. Sutherland, and H. Navelet, Phys. Rep. **228**, 93 (1993), and references therein.
  - [3] M. Ciuchini, E. Franco, G. Martinelli, L. Reina, and L. Silvestrini, Phys. Lett. B **316**, 127 (1993).
  - [4] B. Grinstein and M. B. Wise, Phys. Lett. B **201**, 274 (1988); W.-S. Hou and R. Willey, *ibid.* **202**, 591 (1988); A. J. Buras, P. Krawczyk, M. E. Lautenbacher, and C. Salazar, Nucl. Phys. **B337**, 284 (1990); J. L. Hewett, Phys. Rev. Lett. **70**, 1045 (1993).
  - [5] S. Bertolini, F. Borzumati, A. Masiero, and G. Ridolfi, Nucl. Phys. **B353**, 591 (1991); R. Barbieri and G. F. Giudice, Phys. Lett. B **309**, 86 (1993); J. L. Lopez, D. V. Nanopoulos, and G. T. Park, Phys. Rev. D **48**, 974 (1993).
  - [6] L. Randall and R. Sundrum, Phys. Lett. B **312**, 148 (1993).
  - [7] R. N. Mohapatra and J. C. Pati, Phys. Rev. D **11**, 566 (1975); **11**, 2558 (1975); R. N. Mohapatra and G. Senjanovic, *ibid.* **12**, 1502 (1975).
  - [8] G. Senjanovic, Nucl. Phys. **B153**, 334 (1979).
  - [9] W. Grimus, Report No. UWTHPh-1993-10 (unpublished), and references therein.
  - [10] D. Cocolicchio, G. Costa, G. L. Fogli, J. H. Kim, and A. Masiero, Phys. Rev. D **40**, 1477 (1989).
  - [11] G. M. Asatryan and A. N. Ioannisyian, Yad. Fiz. **51**, 1350 (1990) [Sov. J. Nucl. Phys. **51**, 858 (1990)].
  - [12] P. Langacker, in *CP Violation*, edited by C. Jarlskog (World Scientific, Singapore, 1989), p. 552.
  - [13] P. Langacker and S. U. Sankar, Phys. Rev. D **40**, 1569 (1989).
  - [14] G. Beall, M. Bander, and A. Soni, Phys. Rev. Lett. **48**, 848 (1982).
  - [15] L. Abott, Nucl. Phys. **B185**, 189 (1981).
  - [16] P. Cho and B. Grinstein, Nucl. Phys. **B365**, 279 (1991).
  - [17] T. Inami and C. S. Lim, Prog. Theor. Phys. **65**, 297 (1981); **65**, 1772(E) (1981).
  - [18] N. Cabibbo and L. Maiani, Phys. Lett. **79B**, 109 (1978).
  - [19] M. Misiak, Phys. Lett. B **321**, 113 (1994).
  - [20] D0 Collaboration, S. Abachi *et al.*, Phys. Rev. Lett. **72**, 2138 (1994).
  - [21] K. Fujikawa and A. Yamada, Phys. Rev. D **49**, 5890 (1994).